SAND2011-3709C
Proceedings of ASME 2011 5th International Conference on Energy Sustainability & 9th Fuel Cell Science, Engineering and Technology Conference
ESFuelCell2011
August 7-10, 2011, Washington, DC, USA

ESFuelCell2011-54430

CFD SIMULATION AND PERFORMANCE ANALYSIS OF ALTERNATIVE DESIGNS FOR HIGH-TEMPERATURE SOLID PARTICLE RECEIVERS

Siri Sahib S. Khalsa[1], Joshua M. Christian[2], Gregory J. Kolb[2], Marc Röger[3], Lars Amsbeck[4], Clifford K. Ho[2], Nathan P. Siegel[2], Adam C. Moya[2]

[1]Sandia Staffing Alliance, Sandia National Laboratories, Concentrating Solar Technologies Department, Albuquerque, NM, USA
[2]Sandia National Laboratories, Concentrating Solar Technologies Department, Albuquerque, NM, USA
[3]German Aerospace Center (DLR), Solar Research, Plataforma Solar de Almería, Spain
[4]German Aerospace Center (DLR), Solar Research, Stuttgart, Germany

ABSTRACT

Direct-absorption solid particle receivers are theoretically capable of yielding temperatures in excess of 1000°C, which enables higher efficiency power cycles and lower thermal storage costs. This paper presents rigorous CFD simulations of alternative solid particle receiver designs with recirculation to help identify optimal configurations that maximize the receiver thermal efficiency. The alternative receiver designs considered are a north-facing cavity receiver and a face-down surround-field cavity receiver. The CFD simulations model incident solar radiation from a heliostat field as a boundary condition on the model domain. The CFD simulations also couple convective flow with the thermal and discrete-phase (particle) solutions, which in turn affects absorption of incident solar radiation and thermal re-radiation within the receiver. The receivers are optimized to yield comparable particle temperatures at the outlets of 750-850°C, heated from an injection temperature of 300°C, and are compared on the basis of thermal efficiency. The CFD simulations yielded thermal efficiencies of the north-facing receiver at 72.3% (losses were 6.5% radiative and 20.9% convective) and the face-down receiver at 78.9% (losses were 11.4% radiative and 9.6% convective) at solar noon on March 22. Ongoing efforts are focused on reducing convective and radiative losses from both receiver configurations.

1. INTRODUCTION

Solid particle receivers, which are direct-absorption central receivers that use solid particles as an absorption medium, are theoretically capable of yielding temperatures in excess of 1000°C [1]. These temperatures exceed the stability limit of current nitrate-salt heat-transfer-fluid formulations [2]. The use of higher-temperature central receivers can enable higher efficiency high-temperature power cycles and reduce the costs of thermal storage [3].

Röger et al. [4] evaluated face-down solid particle receivers using analytical models in Matlab. However, these studies did not rigorously model convection due to thermal buoyancy and particle entrainment. Ho et al. [5] developed computational fluid dynamics (CFD) models of a prototype solid particle receiver, which was not optimized and had high convective and radiative losses with no particle recirculation. This paper presents rigorous CFD simulations of alternative solid particle receiver designs with recirculation to help identify optimal configurations that maximize the receiver thermal efficiency. The alternative receiver designs considered are a north-facing cavity receiver and a face-down surround-field cavity receiver.

The CFD simulations model incident solar radiation from a heliostat field as a boundary condition on the model domain, using the method developed by Khalsa and Ho [6]. The CFD simulations also couple convective flow with the thermal and discrete-phase (particle) solutions, which in turn affects absorption of incident solar radiation and thermal re-radiation within the receiver. The receivers are optimized to yield comparable particle temperatures at the outlets, and are compared on the basis of thermal efficiency.

2. OPTIMIZATION OF RECEIVERS AND HELIOSTAT FIELDS

The code DELSOL [7] was used to optimize the heliostat field layouts and receiver aperture dimensions for both the north-facing and face-down receivers. The optimizations considered annual performance and were designed to minimize the

levelized cost of energy (LCOE), as defined by DELSOL. The assumptions used for the optimizations are listed in Table 1.

Table 1. Assumptions for optimization of receivers and heliostat fields [4].

Heliostat Costs	\$177 /m^2
Tower Costs[1]	\$557,000 x exp(1.2·h_T/110m)
Receiver Cost	\$109,000 /MWth
Land Cost	\$3 /m^2
Annuity	0.0988
O&M Costs	2 %/year of total investment
Heliostat Reflective Area	121 m^2 per heliostat (11m x 11m)
Heliostat Reflectivity	0.87
Heliostat Slope Error	1.835 mrad (mirror normal)
Heliostat Facet Canting	All canted to slant range
Receiver Aperture Shape	Rectangular
Required Peak Output	350 MWth
Site Latitude	34.5°N

[1] h_T: tower height in m

DELSOL does not rigorously calculate radiative or convective losses from the receiver, and requires a total W/m^2 loss through the aperture as input in order to perform the optimization. Losses obtained from preliminary CFD results were used as a starting point for the optimization. The optimization results and losses were then iterated between DELSOL and the CFD code in order to converge on an optimum set of parameters, which are listed in Table 2. The north-field for the north-facing receiver and the surround-field for the face-down receiver are plotted in Fig. 1 and Fig. 2, respectively.

Table 2. Receiver and heliostat field parameters yielded by optimizations in DELSOL and the CFD code.

	North-Facing Receiver	**Face-Down Receiver**
Field Type	North	Surround
Power into Receiver at Solar Noon	487 MWth	417 MWth
Number of Heliostats	7,183	5,922
Tower Height	290 m	280 m
Aperture Nod Angle (Down from Horizontal)	20°	90° (face-down)
Aperture Size	17m x 17m	18m x 18m

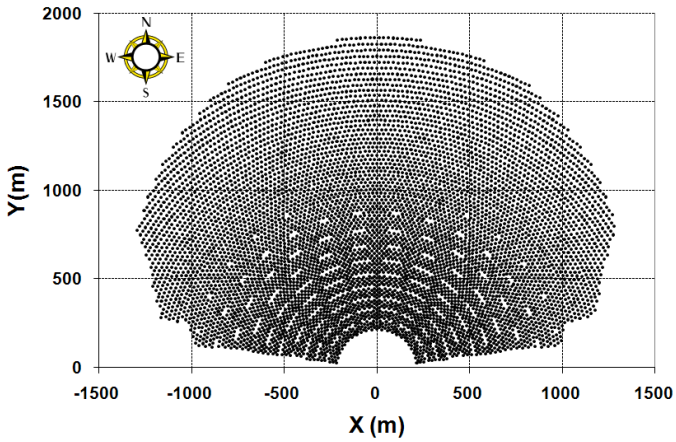

Fig. 1. Plot of the 7,183-heliostat north-field, which delivers 487 MWth into the north-facing cavity receiver at solar noon.

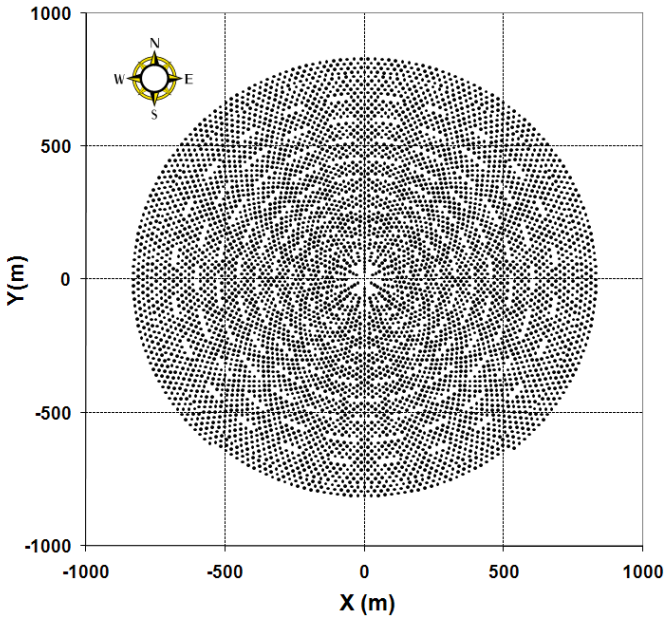

Fig. 2. Plot of the 5,922-heliostat surround-field, which delivers 417 MWth into the face-down cavity receiver at solar noon.

The heliostat field layouts and receiver aperture dimensions yielded by the optimizations were used to design the 3D geometry for each receiver. The geometry for the face-down receiver is shown in Fig. 3. The height of the face-down receiver is equal to the width of the aperture, as per the recommendation of Röger et al. [4]. The geometry for the north-facing receiver is shown in Fig. 4. The particles are injected into the north-facing receiver along a line located 13.0m above the upper edge of the aperture, in order to minimize the fraction of incident solar radiation that strikes a receiver wall before striking the particles. For both receivers, the particles are collected as close to the base of the aperture as possible in order to minimize cooling after the particles fall below the beam.

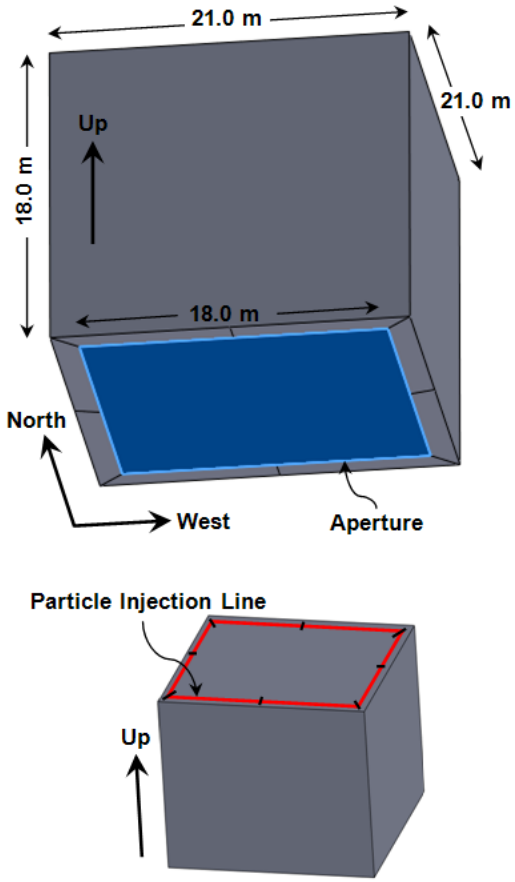

Fig. 3. Face-down cavity receiver with a square aperture. Optimum aperture size was found to be 18m x 18m. Top: receiver as seen from observer on ground. Bottom: particle injection line shown along top face of receiver.

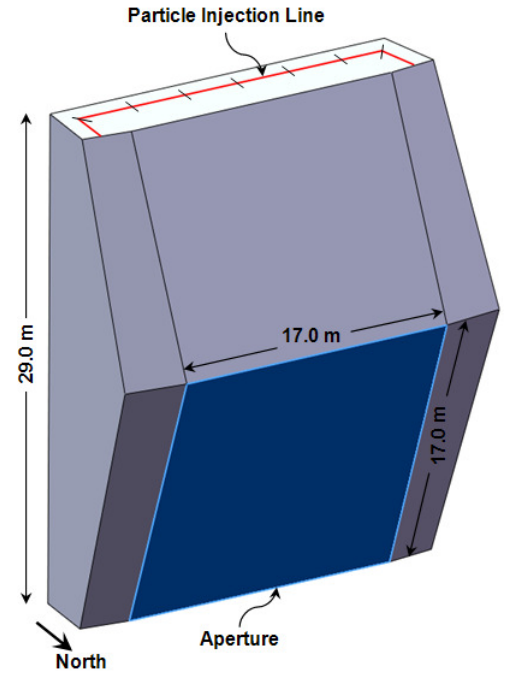

Fig. 4. North-facing cavity receiver with a square aperture. Optimum aperture nod angle and size were found to be 20° down from the horizontal and 17m x 17m, respectively.

3. COMPUTATIONAL FLUID DYNAMICS MODELS

The CFD analysis was performed using ANSYS FLUENT 12.1 (www.fluent.com). The CFD simulation domain was limited to the receiver alone, in order to use the highest resolution possible for the coupled physics within the receiver.

The meshes for both receivers consisted of boundary layers of hexahedral elements along the receiver walls and tetrahedral elements for the majority of the domain interior. A grid convergence study was performed to ensure the meshes chosen for the analysis were sufficiently refined. The total cell counts for the chosen north-facing and face-down receiver meshes were 993,330 and 893,975, respectively. When the mesh refinement was doubled, yielding twice the number of cells, the radiative and convective losses calculated by the CFD simulation each changed by less than 0.3%.

The concentrated radiation from the heliostat field was applied as a collection of radiance boundary conditions across the entire aperture surface, using the method developed by Khalsa and Ho [6]. The radiance boundary conditions honored both the directional and spatial variability across the aperture of the incoming radiance distribution from the heliostat field. The flux distributions on both the north-facing and face-down receiver apertures were calculated by DELSOL and discretized into 121 quadrilateral 'macroelements'. The non-uniform radiant intensity distributions were calculated using the analytical method described in [6]. Each macroelement on the north-facing aperture was further discretized into 9 'microelements', each of which irradiated a unique solid angle within the receiver. Each macroelement on the face-down receiver was discretized into 18 microelements to account for the larger solid angle irradiated by the surround-field.

The solution was solved at steady-state by repeatedly iterating between a radiation-only cycle and a cycle that solved for flow, turbulence, and energy, until a complete energy-balance and mass-balance were achieved. During the flow, turbulence, and energy cycle, a zero-gauge pressure boundary condition that specified a 1.5% turbulent intensity was applied across the entire aperture for both receivers. Any air that flowed into the receiver from the atmosphere was assumed to have a temperature of 300K.

The physical properties of the solid particles that comprise the discrete-phase direct-absorption medium in the CFD model are listed in Table 3.

Table 3. Particle properties used in CFD simulation [4],[5].

Density	3550 kg/m^3
Specific Heat (J/kg/K)	$-7.309\text{x}10^{-4}T^2 + 1.608T + 372.4$, *for* $273 < T \leq 1173K$ 1255, *for* $T > 1173K$
Thermal Conductivity	2.0 W/m/K
Emissivity	0.93
Scattering Factor [9]	0.3
Mean Diameter	697 μm

An analytical model developed in Matlab by Röger et al. [4] was used to estimate the total mass flow rate of particles and the particle recirculation pattern necessary to achieve a particle equilibrium temperature of 750-850°C at the outlet of each receiver, for an injection temperature of 300°C. The required mass flow rates were estimated to be 582 kg/s and 596 kg/s for the north-facing and face-down receivers, respectively. The optimum recirculation pattern for both receivers is illustrated in Fig. 5. The particles are first passed through a pre-heating region of the receiver, where the incident solar flux is relatively low. These pre-heated particles are then recirculated to the peak-flux region of the receiver, before falling into hoppers at the base of the receiver.

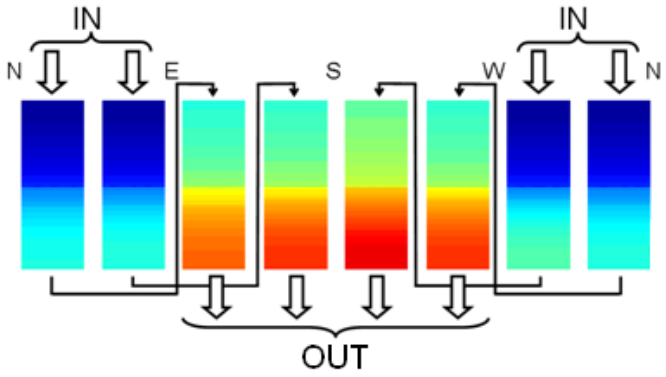

Fig. 5. Optimum particle recirculation pattern for both the north-facing and face-down receivers at solar noon. From [4].

The walls of both receivers were simulated as the diffusely-reflecting material Duraboard HD with emissivities 0.2 (wavelength, $\lambda < 4.5\mu m$) and 0.8 ($\lambda > 4.5\mu m$) [8].

The radiation solution was solved using a 2-band Discrete Ordinates radiation model (band 1: $\lambda < 4.5\mu m$; band 2: $\lambda > 4.5\mu m$). The θ x φ angular discretization and pixelation (see [9]) were set to 10 x 10 and 3 x 3, respectively. Previous work [6] has shown that these angular discretization and pixelation values are suitable to yield sufficiently accurate radiation distributions within the receiver. The flow solution was coupled to a realizable k-ε turbulence model with a standard wall function [8]. The discrete-phase (particle) solutions for the radiation, flow, turbulence, and energy equations were coupled to those of the continuous phase (air).

4. RESULTS AND ANALYSIS

The simulations of both receivers converged with energy imbalances of less than 0.4%. The particle equilibrium temperatures at the outlets of the north-facing and face-down receivers were 819°C and 769°C, respectively at solar noon on March 22. The particle equilibrium temperature at the outlet is defined as the temperature that all the particles at the outlet would attain if they were allowed to reach thermal equilibrium with each other. Both of these temperatures fall within the target range of 750-850°C, and it is assumed that the difference between these equilibrium temperatures is sufficiently low to provide a valid basis for comparison of the receiver losses and efficiencies.

The effectiveness of the recirculation pattern is illustrated in the plot of particle tracks in the north-facing receiver (Fig. 6). The outer particle injections are preheated to ~520°C before they are recirculated toward the center of the receiver, where they reach temperatures as high as 919°C.

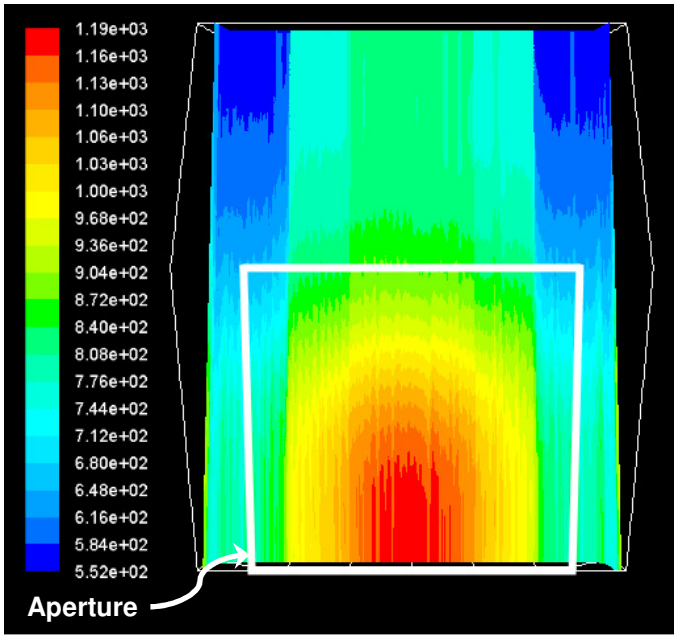

Fig. 6. Particle tracks through the north-facing receiver at solar noon, colored by particle temperature (K).

The distributions of particle temperatures at the outlets of the north-facing and face-down receivers are displayed as histograms in Fig. 7 and Fig. 8. The standard deviations of particle temperatures at the outlets of the north-facing and face-down receivers are 73°C and 35°C, respectively.

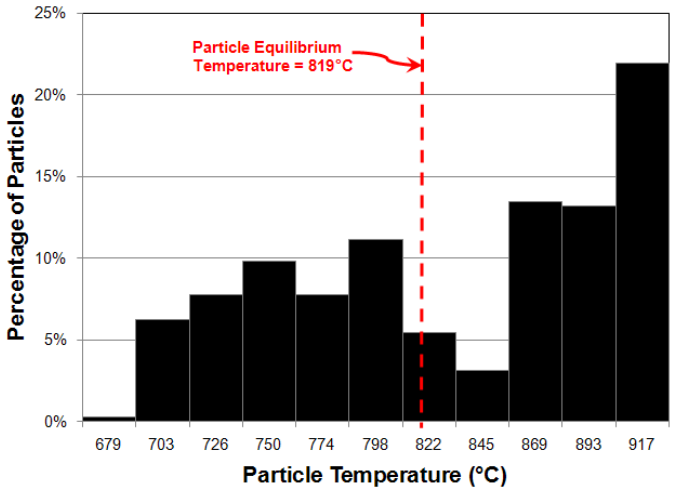

Fig. 7. Histogram of particle temperatures at the outlet of the north-facing receiver at solar noon.

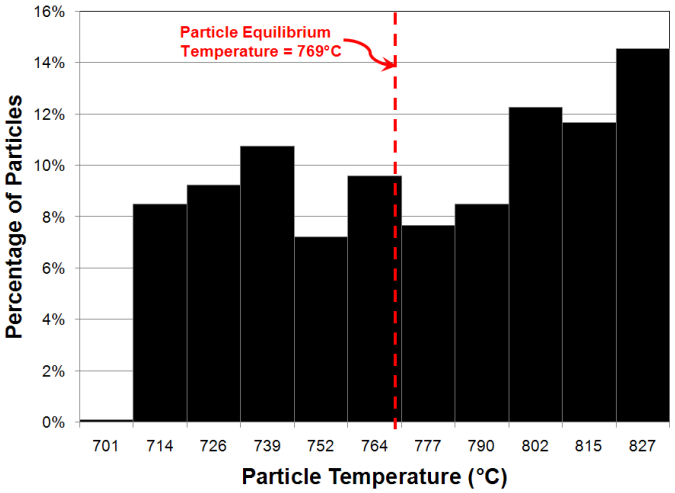

Fig. 8. Histogram of particle temperatures at the outlet of the face-down receiver at solar noon.

The overall losses and efficiencies calculated by the CFD simulations are displayed in Table 4. Thermal Efficiency is defined as the net power absorbed by the particles as a fraction of the total input power.

Table 4. Performance comparison of north-facing and face-down receivers at solar noon on March 22, as calculated by the CFD simulations.

	North-Facing Receiver	Face-Down Receiver
Particle Injection Temperature	300°C	300°C
Particle Equilibrium Temperature at Outlet	819°C	769°C
Radiative Losses	6.5%	11.4%
Convective Losses	20.9%	9.6%
Thermal Efficiency	72.3%	78.9%

Convective losses predominate in the north-facing receiver, whereas radiative losses predominate in the face-down receiver. The reasons for the higher convective losses in the north-facing receiver are revealed by vector plots of the air flow patterns in the receivers (Fig. 9 and Fig. 10). In the north-facing receiver, the particles entrain hot air and force the hot air to escape at the base of the receiver. Cool air from the atmosphere is consequently pulled into the receiver from the upper region of aperture, allowing the cool air to fall along and remove heat from almost the entire length of the particle curtain, before it is ejected as hot air at the base of the aperture.

In the face-down receiver, although the particle curtain also entrains air toward the base of the receiver, cool air from the atmosphere must enter the receiver at the base of the receiver due to its face-down orientation. This results in a localization of the cool ambient air near the base of the receiver, thereby limiting its ability to remove heat from the particles.

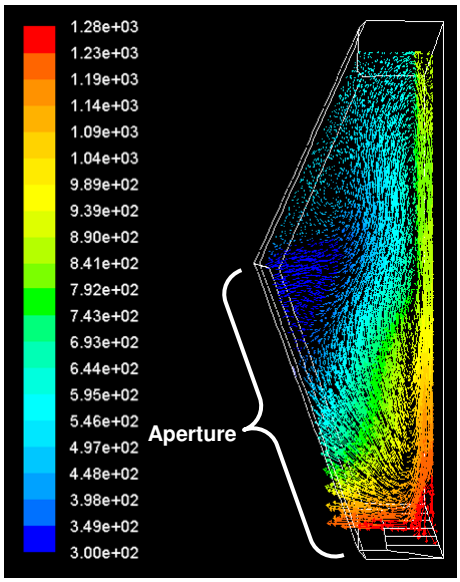

Fig. 9. Air velocity vectors along a plane in the north-facing receiver at solar noon, colored by air temperature (K).

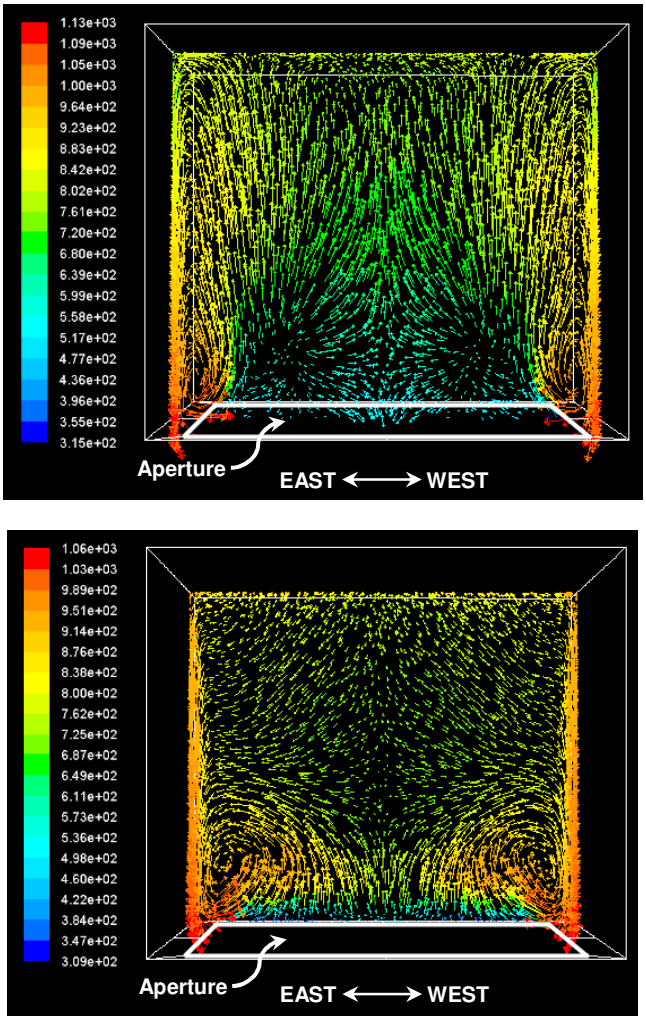

Fig. 10. Air velocity vectors along planes in the face-down receiver at solar noon, colored by air temperature (K). Top: plane located at the aperture center. Bottom: plane located 7.5m south of the aperture center.

The convective losses calculated by the CFD simulations are most likely upper-bounds to the potential convective losses from these receivers, because any air that entered the receiver from the atmosphere was assumed to have a temperature of 300K. Under non-windy conditions, the air immediately outside the aperture would be a mixture of ambient-temperature air and hot air expelled from the receiver, resulting in air with temperatures notably higher than 300K entering the receiver. However, under windy conditions this hotter air mixture would likely be swept away, resulting in ambient-temperature air predominating the volume immediately outside the aperture.

The higher radiative losses in the face-down receiver may be due to the lower opacity of its particle curtains relative to those of the north-facing receiver. Each of the 8 curtains in the face-down receiver flows at a rate of 148.9 kg/s spread over an injection length of 10.0 m. Each of the 8 curtains curtain in the north-facing receiver flows at a rate of 145.5 kg/s spread over an injection length 3.3 m. Therefore, the mass flow rate per unit length (kg/s-m) of the particle curtains in the face-down receiver is 66% less than in the north-facing receiver. The resulting particle curtain opacities were calculated using results from the CFD simulations and Eq. 1 [10]:

$$\text{Opacity} = 1 - e^{\frac{-3fw}{2d}} \quad (1)$$

where f is the particle volume fraction, w is the particle curtain thickness, and d is the particle diameter. The calculated particle curtain opacities were 76.1% for the face-down receiver and 98.6% for the north-facing receiver along planes located at half the receiver height. The lower opacity of the particle curtains in the face-down receiver results in reduced absorption of incident and reflected concentrated solar radiation and thermal emissions from the hot cavity walls, thereby increasing radiative losses.

Ongoing efforts are focused on reducing losses from both receiver configurations. An optimal balance would need to be determined for the proposed improvements in order to mitigate potentially negative effects associated with their implementation. Convective losses from the north-facing receiver may be reduced by increasing the aperture nod angle away from the vertical, based on the results of this study. Radiative and convective losses from both receivers may be mitigated by reducing the aperture size. Both of these modifications could increase beam spillage, however. Convective losses from both receivers might be reduced by dropping the particle curtains farther from the aperture. This may also reduce the concentrated solar flux incident on the particle curtains and increase radiative losses due to reflections from the side walls. Chen et al. [11] and Siegel et al. [8] show that increasing the curtain opacity by increasing the particle mass flow rate mitigates radiative losses from the receiver, but also reduces the particle outlet temperatures for a given input power. An effective use of particle recirculation patterns might allow for an increase in curtain opacity without reducing particle outlet temperatures, as described by Röger et al. [4]. Chen et al. [11] predict that both the overall receiver efficiency and particle outlet temperatures could be increased by reducing the particle diameter. There may be a minimum diameter that is feasible for a particular receiver, as a reduction in particle diameter may increase the susceptibility of particles to be swept out of the receiver by external winds and convective flow. In order to mitigate particle loss and convective losses due to external winds, Kolb [12] proposes a "suction-recirculation" device that injects air from the aperture-side of a north-facing receiver and pulls air through holes in the back wall. Tan et al. [13] suggest that an air curtain ("aerowindow") over the aperture formed using air jets could reduce convective losses from a north-facing receiver in the presence of wind.

5. CONCLUSIONS

This paper presented rigorous CFD simulations of alternative solid particle receiver designs with particle recirculation to help identify optimal configurations that maximize the receiver thermal efficiency. The alternative receiver designs considered were a north-facing cavity receiver and a face-down surround-field cavity receiver. The CFD simulations modeled incident solar radiation from a heliostat field as a boundary condition on the model domain. The CFD simulations also coupled convective flow with the thermal and discrete-phase (particle) solutions, which in turn affected absorption of incident solar radiation and thermal re-radiation within the receiver. The receivers were optimized using DELSOL, an analytical Matlab code, and the CFD code ANSYS FLUENT to yield comparable particle temperatures at the outlets, and were compared on the basis of thermal efficiency.

The CFD simulations yielded thermal efficiencies of the north-facing receiver at 72.3% (losses were 6.5% radiative and 20.9% convective) and the face-down receiver at 78.9% (losses were 11.4% radiative and 9.6% convective) at solar noon on March 22. Ongoing efforts are focused on reducing convective and radiative losses from both receiver configurations, and studying their performance at part-load conditions.

ACKNOWLEDGMENTS

The authors thank Bill Arnold (Sandia National Laboratories) for his assistance and initial analyses of the recirculation patterns.

Sandia National Laboratories is a multi-program laboratory managed and operated by Sandia Corporation, a wholly owned subsidiary of Lockheed Martin Corporation, for the U.S. Department of Energy's National Nuclear Security Administration under contract DE-AC04-94AL85000.

published form of this work, or allow others to do so, for United States Government purposes.

REFERENCES

[1] Hruby, J.M. 1986. "A Technical Feasibility Study of a Solid Particle Solar Central Receiver for High Temperature Applications". Sandia National Laboratories, Albuquerque, NM, SAND86-8211.

[2] Carling, R.W. and R.W. Bradshaw. 1987. "A Review of the Chemical and Physical Properties of Molten Alkali Nitrate Salts and Their Effect on Materials Used For Solar Central Receivers". Sandia National Laboratories, Albuquerque, NM, SAND87-8005.

[3] Moore, R., M. Vernon, C.K. Ho, N.P. Siegel, and G.J. Kolb. 2010. "Design Considerations for Concentrating Solar Power Tower Systems Employing Molten Salt". Sandia National Laboratories, Albuquerque, NM, SAND2010-6978.

[4] Röger, M., L. Amsbeck, B. Gobereit, and R. Buck. 2011. "Face-Down Solid Particle Receiver Using Recirculation". In press, J. Sol. Energy Eng.

[5] Ho, C.K., M. Röger, S.S. Khalsa, L. Amsbeck, R. Buck, N.P. Siegel, and G.J. Kolb. 2009. "Experimental Validation of Different Modeling Approaches for Solid Particle Receivers". SolarPACES 2009, Berlin, Germany, September 15-18, 2009.

[6] Khalsa, S.S. and C.K. Ho. 2011. "Radiation Boundary Conditions for Computational Fluid Dynamics Models of High-Temperature Cavity Receivers". In press, J. Sol. Energy Eng.

[7] Kistler, B.L. 1986. "A User's Manual for DELSOL3: A Computer Code for Calculating the Optical Performance and Optimal System Design for Solar Thermal Central Receiver Plants". Sandia National Laboratories, Albuquerque, NM, SAND86-8018.

[8] Siegel, N.P., C.K. Ho, S.S. Khalsa, and G.J. Kolb. 2010. "Development and Evaluation of a Prototype Solid Particle Receiver: On-Sun Testing and Model Validation". J. Sol. Energy Eng., *132* (2), 021008, DOI:10.1115/1.4001146

[9] ANSYS, Inc. 2009. "ANSYS FLUENT 12.0 Theory Guide". ANSYS, Inc., Canonsburg, PA.

[10] Siegel, N., G. Kolb, K. Kim, V. Rangaswamy, and S. Moujaes. 2007. "Solid Particle Receiver Flow Characterization Studies." Proceedings of ASME Energy Sustainability 2007, Long Beach, CA, June 20-27, 2007, ES2007-36118.

[11] Chen, H., Y. Chen, H. Hsieh, and N. Siegel. 2007. "Computational Fluid Dynamics Modeling of Gas-Particle Flow Within a Solid-Particle Solar Receiver." J. Sol. Energy Eng., *129* (2), 160-170, DOI:10.1115/1.2716418

[12] Kolb, G. 2009. "Suction-Recirculation Device for Stabilizing Particle Flows Within a Solar Powered Solid Particle Receiver." Patent Application SD-10824, Sandia National Laboratories, Albuquerque, NM.

[13] Tan, T., Y. Chen, Z. Chen, N. Siegel, and G.J. Kolb. 2009. "Wind Effect on the Performance of Solid Particle Solar Receivers With and Without the Protection of an Aerowindow." J. Sol. Energy, *83* (10), 1815-1827, DOI:10.1016/j.solener.2009.06.014